On-line Inertia Estimation for Synchronous and Non-Synchronous Devices

Muyang Liu, *Member, IEEE*, Junru Chen, *Member, IEEE*, Federico Milano, *Fellow, IEEE*

***Abstract*— This paper proposes an on-line estimation method able to track the inertia of synchronous machines as well as the equivalent, possibly time-varying inertia from the converter-interfaced generators. For power electronics devices, the droop gain of the Fast Frequency Response (FFR) is also determined as a byproduct of the inertia estimation. The proposed method is shown to be robust against noise and to track accurately the inertia of synchronous generators, virtual synchronous generators with constant and adaptive inertia, and wind power plants with inclusion of energy storage-based frequency control.**

***Index Terms*— Inertia estimation, power system dynamics, Fast Frequency Response (FFR), equivalent inertia, Converter-Interfaced Generation (CIG).**

I. Introduction

A. Motivation

The replacement of Synchronous Generators (SGs) with non-synchronous devices, namely Converter-Interfaced Generation (CIG) sources, such as wind and solar, decreases the inertia of the power system [1]. This creates operation and security issues as a minimum inertia is required in the system [2]. Advanced control schemes that make non-synchronous devices provide inertia support have been developed in recent year. Examples are the virtual synchronous generator control [3] and inertial response control [4]. The objective of these controls is to emulate the inertia response in the SGs and thus enforce the non-synchronous devices boosting the power at the instant of the contingency, and therefore, leading to the concept of equivalent inertia. The equivalent inertia of non-synchronous devices, unlike the inertia constant of SG, may be variable [5], and even be specially designed as time-varying [6]. A general method to fast and accurately estimate both the constant and non-constant (equivalent) inertia, however, is still missing. This paper aims at developing an on-line inertia estimation method that can accurately track the (equivalent) inertia of both synchronous and non-synchronous devices.

B. Literature Review

Efforts have been made to improve the accuracy to estimate the inertia constant for SGs via off-line tests [7]–[9]. Similar techniques also developed for the off-line identification for the inertia of non-synchronous renewable turbines [10], [11]. The inertia of these devices can be uncertain, or even time-varying, due to the ever-changing renewables and converter controls [12]. Off-line tests, therefore, are not enough to track the presented inertia of the non-synchronous devices.

The accurate and precise on-line monitoring for the dynamic behavior of the power system becomes feasible with the development of the smart grid techniques [13], especially, the wide application of Phasor Measurement Units (PMUs) [8], [14]. For example, reference [15] presents a Bayesian framework based on the data collected with PMUs to estimate the inertia of the generators with high accuracy. The high computational burden of the Bayesian method, however, makes its utilization impractical for on-line monitoring. Several PMU-based estimation methods for the equivalent inertia constant of a power system have been developed [16]–[19]. Most of them, however, are not adequate tools for the on-line inertia estimation of single devices, especially non-synchronous devices with non-constant inertia control.

Reference [16] proposes an on-line identification algorithm for the equivalent inertia of an entire power system by analyzing its dynamic response to a designed microperturbation. Since the microperturbation signal affects the frequency response of the system, it may lead to the unexceptional action of the protective relays and thus increases the potential risk of the power system stability. The same limit also exists for the perturbation-needed inertia estimation method proposed in [17]. Reference [18] obtains the system inertia by analyzing the frequency signal via rotational invariance techniques. The analysis requires a precise model that may not be available in real-world applications. Reference [19] avoids the limitations of [16]–[18] by proposing an on-line inertia estimator based on the extension and mixture of a dynamic regressor. While this regressor is designed under the assumption that the inertia is constant. Time-varying equivalent inertia, therefore, can prevent above estimation techniques to converge.

C. Contributions

This paper takes inspiration from the inertia estimation formula proposed in [20] and [21], which is able to on-line track the physical or equivalent inertia of a device. Such a formula, however, is prone to numerical issues. With this regard, the specific contributions of this work are the following:

- A discussion of the numerical issues of the inertia estimation formula proposed in [20], [21] and the proposal of two new formulas with improved numerical stability.
- As a byproduct of the above, a formula able to estimate, under certain conditions, the damping of SGs and the droop gain of FFR controls.

The authors are with AMPSAS, School of Electrical and Electronic Engineering, University College Dublin, Ireland. E-mails: muyang.liu@ucd.ie, junru.chen.1@ucdconnect.ie, and federico.milano@ucd.ie).

This work is supported by the Science Foundation Ireland, by funding Muyang Liu and Federico Milano under the Investigator Program Grant No. SFI/15/IA/3074; and by the European commission, by funding Junru Chen and Federico Milano under the project EdgeFLEX, Grant No. 883710.

- The design of on-line inertia estimators that are based on the proposed formulas.

The accuracy of the inertia estimators on tracking the constant or non-constant inertia of synchronous and non-synchronous devices is duly tested via the revised WSCC 9-bus system under several scenarios.

D. Organization

The remainder of the paper is organized as follows. Section II reviews the basic concepts developed in [20] and leads to the on-line inertia estimation discussed in this paper. Section III proposes the improved inertia estimation methods with higher accuracy. The WSCC 9-bus system, adequately modified to include non-synchronous generation, serves to investigate the performance of the proposed inertia estimators on different devices, including SG, Virtual Synchronous Generator (VSG) and Wind Power Plant (WPP). Conclusions are drawn in Section V.

II. Technical Background

Subsection II-A recalls the definition of the inertia constant of SG and outlines the frequency evaluation of the power system dominated by SGs. Subsection II-B presents the developed inertia estimation formula of [20] and [21] and discusses its numerical issues.

A. Inertia constant and system frequency evaluation

The inertia constant conditions the dynamic of SGs through the well-known swing equation:

$$M_G\,\dot{\omega}_G = p_m - p_G - D_G\,(\omega_G - \omega_o)\;, \tag{1}$$

where ω_G is the rotor speed of the SG; ω_o is the reference angular speed; D_G is the damping; M_G is the mechanical starting time; p_G is the electrical power of the SG injected into the grid; and p_m is the mechanical power of the SG. The inertia constant is defined as $H_G = M_G/2$ [22]. To avoid carrying around the factor "2", the estimation technique described in the remainder of this paper are aimed at determining M_G.

For the derivation of the inertia estimation formula discussed in the next section, it is convenient to split the mechanical power into three components:

$$p_m = p_{\rm UC} + p_{\rm PFC} + p_{\rm SFC}\;, \tag{2}$$

where $p_{\rm UC}$ is the power set point obtained by solving of the unit commitment problem; $p_{\rm PFC}$ is the active power regulated by the Primary Frequency Control (PFC) and $p_{\rm SFC}$ is the active power regulated by the Secondary Frequency Control (SFC). For a typical SG, the PFC is achieved through Turbine Governor (TG), and the SFC is achieved through Automatic Generation Control (AGC).

Figure 1 shows a typical frequency evolution of a power system following a contingency [23]. As we can see in Fig. 1, the evolution of the frequency can be divided into three time scales, namely the inertial response, the PFC and the SFC. These time scales differ by an order of magnitude from each other: $T_{\rm inertia} \approx 1$ s, $T_{\rm PFC} \approx 10$ s and $T_{\rm SFC} \approx 100$ s.

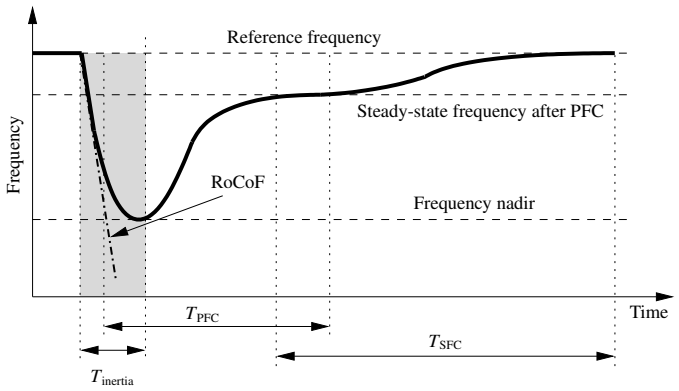

Fig. 1: Time scales of the frequency response and regulation of synchronous machines.

During the period of inertial response, the dynamic behavior of the frequency mainly depends on the inertia of the system and is characterized by a relatively high $\dot{\omega}$, often called Rate of Change of Frequency (RoCoF) [24]. Following the inertial response, the frequency gradually recovers to the nominal via the PFC and SFC. The inertia estimation approach proposed in this paper takes advantage of the fact that the inertial response is the fastest among the frequency response of the synchronous machine and the one with highest $\dot{\omega}$.

B. Existing inertia estimation formulation

Differentiating (1) with respect to time and taking into account (2), we can deduce:

$$M_G\,\ddot{\omega}_G = \dot{p}_{\rm UC} + \dot{p}_{\rm PFC} + \dot{p}_{\rm SFC} - \dot{p}_G - D_G\,\dot{\omega}_G\;. \tag{3}$$

Within the inertial response time scale, we can assume that:

$$\dot{p}_{\rm UC} \approx 0,\;\; \dot{p}_{\rm SFC} \approx 0\;, \tag{4}$$

and:

$$|\dot{p}_{\rm PFC}| \ll |\dot{p}_G|\;. \tag{5}$$

Since p_G is the SG grid power injection, it is always measurable by the Transmission System Operators (TSOs). Then, reference [20] discusses how to estimate $\dot{p}_G$, abbreviated as Rate of Change of Power (RoCoP), based on PMUs measurements. Finally, based on the estimation technique proposed in [25], we can assume to be able to estimate ω_G and, thus, be able to calculate $\ddot{\omega}_G$. In the following, we can thus assume that $\dot{p}_G$ and $\ddot{\omega}_G$ are measurable and known.

With these assumptions, the inertia estimation formula is proposed as a byproduct of the RoCoP:

$$M_G \approx M_G^* = -\frac{\dot{p}_G}{\ddot{\omega}_G}\;, \tag{6}$$

where $*$ indicates an estimated quantities and it is further assumed that $\dot{p}_{\rm PFC} \approx 0$ and $D_G \approx 0$. The former assumption holds in the time scale of the inertial response of SG. Note that neglecting the damping and PFC is acceptable for SGs but might not be adequate for non-synchronous devices. With this in mind, Section III-B proposes a method to eliminate the impact of damping and PFC on the inertia estimation of CIG.

Reference [21] extends the estimation formula (6) to evaluate the (equivalent) inertia of *any* device that is able to modify the frequency at its point of connection with the grid, namely those devices whose power injection satisfies the condition:

$$|\dot{p}_{\rm bb}| > \epsilon_p \ , \tag{7}$$

where the subindex bb indicates a *black box* device; and ϵ_p is an empirical threshold to exclude the small frequency fluctuations due to, for example, the stochastic variations of ever-changing renewable sources such as wind and solar generation.

The generalized inertia estimation formula is:

$$M_{\rm bb} \approx M^*_{\rm bb} = -\frac{\dot{p}_{\rm bb}}{\ddot{\omega}_{\rm bb}} \ , \tag{8}$$

where, $\dot{p}_{\rm bb}$ can be obtained through the RoCoP estimation method proposed in [21]; and, according to Frequency Divider Formula (FDF) [26], the internal frequency of the device $\omega_{\rm bb}$ can always be obtained through:

$$\omega_{\rm bb} = \omega_B - x_{\rm eq}\, \dot{p}_{\rm bb} \ , \tag{9}$$

where ω_B is the bus frequency the device connected to, and $x_{\rm eq}$ is the equivalent impedance of the device.

Although (8) proves to be fast and accurate in some scenarios, it may fail due to numerical issues. Equation (8), in fact, utilizes the second derivatives of the frequency signal as the denominator, which might change sign and, thus, cross zero in the first seconds after a contingency and therefore lead to a singularity of (8).

A simple heuristic to remove the singularity consists in holding the current value of the estimated inertia if the denominator is close to zero:

$$M^*_{\rm bb} = \begin{cases} -\dfrac{\dot{p}_{\rm bb}}{\ddot{\omega}_{\rm bb}}, & |\ddot{\omega}_{\rm bb}| \geq \epsilon_o \ , \\ M^*_{\rm bb}(t-\Delta t)\,, & |\ddot{\omega}_{\rm bb}| < \epsilon_o \ , \end{cases} \tag{10}$$

where Δt is the sampling time and ϵ_o is a positive threshold to avoid the numerical issue. In the reminder of this paper, we use (10), rather than (8), to compare the inertia estimation technique proposed in this paper with the one discussed in [25]. A large ϵ_o leads to estimation error, while a small ϵ_o cannot avoid numerical issues. According to a comprehensive set of numerical tests, we have concluded that a proper ϵ_o is hard to find, if it exists at all, and is device dependent. Therefore, in the following section, we propose a new formula with enhanced numerical stability.

III. Proposed On-line Inertia Estimators

This section elaborates on (8) and proposes two novel inertia estimation formulas. The first formula is presented in Subsection III-A and avoids the numerical issue of (8). The second formula is presented in Subsection III-B and accounts for damping and PFC through an additional formula, which can also be utilized to estimate the droop gain of the FFR control of non-synchronous devices, as discussed in Subsection III-C. Finally, Subsection III-D provides the design of the inertia estimators based on the proposed formulas.

A. Improved formula with better numerical stability

As discussed in Section II-B, the fragile numerical stability of (8) is due to the division by $\ddot{\omega}$. Therefore, we propose the following differential equation that avoids such a division:

$$T_M \dot{M}^*_{\rm bb} = \gamma\big(\ddot{\omega}_{\rm bb}\big)\, \big(\dot{p}_{\rm bb} + M^*_{\rm bb}\ddot{\omega}_{\rm bb}\big) \ , \tag{11}$$

where

$$\gamma(x) = \begin{cases} -1\,, & x \geq \epsilon_x \ , \\ 0\,, & -\epsilon_x < x < \epsilon_x \ , \\ 1\,, & x \leq -\epsilon_x \ , \end{cases} \tag{12}$$

and ϵ_x is a small positive threshold closing to zero.

The rationale behind (11) is as follows. At the equilibrium point, $M^*_{\rm bb}\ddot{\omega}_{\rm bb} = -\dot{p}_{\rm bb}$. According to (8), this conditions is obtained for $M^*_{\rm bb} = M_{\rm bb}$, which is the sought inertia value. During a transient, $M^*_{\rm bb}\ddot{\omega}_{\rm bb} \neq -\dot{p}_{\rm bb}$. Let us consider the case $M^*_{\rm bb}\ddot{\omega}_{\rm bb} > -\dot{p}_{\rm bb}$. Then the sign of $\dot{M}^*_{\rm bb}$ is adjusted through the function $\gamma(\ddot{\omega}_{\rm bb})$ in roder to make $M^*_{\rm bb}$ converge to $M_{\rm bb}$. The sign of γ is decided based on the sign of $\ddot{\omega}_{\rm bb}$. If $\ddot{\omega}_{\rm bb} > 0$, $M^*_{\rm bb}$ has to decrease to decrease $M^*_{\rm bb}\ddot{\omega}_{\rm bb}$ and thus $\gamma(\ddot{\omega}_{\rm bb}) = -1$. Otherwise, if $\ddot{\omega}_{\rm bb} < 0$, $\gamma(\ddot{\omega}_{\rm bb}) = 1$ to increase $M^*_{\rm bb}$. The time constant T_M decides the rate of change speed of $M^*_{\rm bb}$. To avoid chattering around the the equilibrium point, a small deadband is included in (12), namely $(-\epsilon_x, \epsilon_x)$. A proper choice of ϵ_x can effectively reduce the impact of frequency fluctuations and noise, and therefore, the deadband for RoCoP, namely (7) is no longer needed.

Compared to (8), the inertia estimation formula (11) not only avoids numerical issues, but also allows filtering spikes and noises by adjusting T_M. Using a proper initial guess on $M^*_{\rm bb}$ can improve the speed of the estimation (11), but it is not essential for convergence. Finally, note that all results presented in this paper are obtained assuming the initial condition $M^*_{\rm bb}(0) = 0$, where $t = 0$ corresponds to the time at which the contingency occurs. This value serves to show that the proposed method is fast, effective and is suitable for on-line applications as it does not require storing historical data. In practice, however, any value of $M^*_{\rm bb}$ as obtained from previous estimations can be used.

B. Improved formula with damping estimation

This subsection focuses exclusively on SGs. The accuracy of (11) can be increased by removing the assumption $D_G \approx 0$. With this in mind, we rewrite (11) as:

$$T_M \dot{M}^*_G = \gamma(\ddot{\omega}_G)\, [\, \dot{p}_G + M^*_G\ddot{\omega}_G + D^*_G\dot{\omega}_G\,] \ , \tag{13}$$

where D^*_G is the estimated value of damping, which is not known. The following equation allows estimating the damping:

$$T_D \dot{D}^*_G = \gamma(\Delta\omega_G)\, [\Delta p_G + M^*_G\dot{\omega}_G + D^*_G\Delta\omega_G] \ , \tag{14}$$

where $\Delta\omega_G = \omega_G - \omega_{G,o}$, with $\omega_{G,o} = \omega_G(0)$, or equivalently:

$$\Delta\omega_G = \int \dot{\omega}_G dt \ , \tag{15}$$

and

$$\Delta p_G = \int \dot{p}_G dt \ . \tag{16}$$

According to (12), the proposed inertia estimation formulas (13)-(14) introduce two thresholds related to the frequency variations of the device, namely $\epsilon_{\ddot{\omega}_G}$ and $\epsilon_{\Delta\omega_G}$. If properly set, these two thresholds can remove small frequency fluctuations resulting from the stochastic renewable energy sources in a more effective way than (7).

Note that even though the integrals in (15) and (16) are presented as indefinite integrals, in practice, they are calculated with a fixed initial time. In particular, $t = 0$ s is used as the initial time when the disturbance that triggers the variations of the frequency occurs, namely at the moment the step change from 0 to ± 1 of the function γ occurs.

The on-line estimator based on (13)-(14) allows to eliminate the impact of damping on the accuracy of inertia estimation. However, the estimated damping D_G^* may never converge to the actual D_G due to the effect of PFC. In the first seconds following a contingency, we have:

$$p_{\mathrm{PFC}} = -R\big(\omega_G - \omega_{\mathrm{ref}}\big) \ , \tag{17}$$

where ω_{ref} is the reference of the frequency, R is the droop gain of TG [22].

Substituting (17) into (3), we have:

$$\dot{p}_G + M_G\ddot{\omega}_G + \big(D_G + R\big)\dot{\omega}_G = 0 \ . \tag{18}$$

Let us consider another reasonable assumption that $\omega_{G,o} \approx \omega_{G,\mathrm{ref}}$. Therefore, one can always assume:

$$\int \dot{\omega}_G dt \approx \omega_G - \omega_{G,\mathrm{ref}} \ . \tag{19}$$

Substituting (17) and (19) into (1), we have:

$$\int \dot{p}_G dt + M_G\dot{\omega}_G + \big(D_G + R\big)\int \dot{\omega}_G dt = 0 \ . \tag{20}$$

Comparing (18)-(20) with (13)-(14), we can deduce that D_G^* in (13) and (14) actually tracks $D_G + R$. Since $\dot{\omega}_G$ varies much slower than $\ddot{\omega}_G$ within the first seconds after a contingency, D_G^* will take more time to converge than M_G^*.

The discussion above proves that D_G^* cannot accurately estimate the damping of SGs but effectively improve the accuracy of inertia estimation by eliminating the impact of damping and PFC through taking their resulted power variations into account.

C. Applications to non-synchronous devices with FFR

Equations (13)-(14) can be generalized for any device that regulates the frequency. Dropping for simplicity the subindex G, we have:

$$T_M\dot{M}^* = \gamma(\ddot{\omega})[\,\dot{p} - M^*\ddot{\omega} - D^*\dot{\omega}\,] \ , \tag{21}$$

$$T_D\dot{D}^* = \gamma\left(\int \dot{\omega}dt\right)\left[\int \dot{p}dt - M^*\dot{\omega} - D^*\int \dot{\omega}dt\right] \ , \tag{22}$$

where ω is the internal frequency of the non-synchronous device.

Note that the time constants T_M and T_D should be small enough to accurately track the time-varying inertia. Small time constants, however, make (21)-(22) more sensitive to noise and may introduce spurious oscillations. This issue can be solved through an additional filter. An example that illustrates this point is given in Section IV-B.

The formulas (21)-(22) can be utilized to obtain the droop gain of the FFR that is modeled as:

$$p_{\mathrm{FFR}} = -R(\omega_{\mathrm{grid}} - \omega_{\mathrm{ref}}) \ , \tag{23}$$

where ω_{grid} is the grid frequency.

Here we should highlight that in contrast to SG, the primary response in CIG is instant along with the inertia response after the contingency. The damping is the friction of the rotational change of the device to the grid frequency, while the droop is the frequency deviation of the grid frequency to the nominal one, as follows:

$$M\,\dot{\omega} = p_{\mathrm{UC}} + p_{\mathrm{FFR}} - p - D\,(\omega - \omega_{\mathrm{grid}}) \ . \tag{24}$$

In CIG, the device tracks the grid frequency change simultaneously, e.g. via the Phase-Locked Loop (PLL) with time constant below 0.1 s. Therefore, we can assume that $\omega \approx \omega_{\mathrm{grid}}$ and accordingly:

$$D\,(\omega - \omega_{\mathrm{grid}}) \ll p_{\mathrm{FFR}} \ . \tag{25}$$

Comparing (25) with (20), we can deduce, for CIG sources, the D^* of the estimator (21)-(22) actually tracks R.

D. Design of real-time loop

The proposed inertia estimation formulas can be used to fulfill the real-time measuring of the inertia through the estimators fed by the RoCoP and RoCoF signals.

Figure 2 shows the structure of a real-time inertia estimator based on (11). If $|\ddot{\omega}| < \epsilon_{\ddot{\omega}}$ in $\gamma(\ddot{\omega})$ (see (12)), $dM^* = 0$ holds. This condition indicates that the estimated M^* can be held after the inertial response with a proper $\epsilon_{\ddot{\omega}}$.

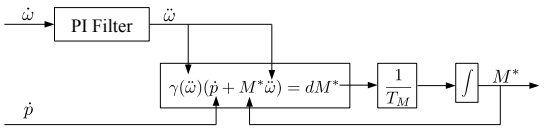

Fig. 2: Real-time loop for inertia estimation (11).

The control scheme of the PI filter included in Fig. 2 is shown by Fig. 3. The parameters of the PI filter are selected as $K_p = 50$, $K_i = 1$ and $T_f = 0.0001$ for all the simulation results shown in the remainder of the paper.

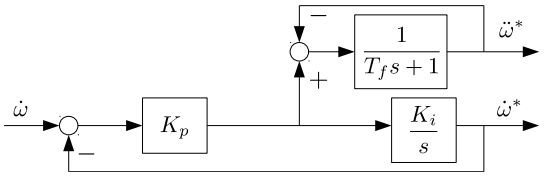

Fig. 3: Control scheme of PI filter.

The real-time loop of the inertia estimator based on (21)-(22) is shown in Fig. 4. Instead of directly taking the input $\dot{\omega}$ for computing dD^*, the $\dot{\omega}^*$ passing through the PI filter improves the robustness of the estimator against measurement noise.

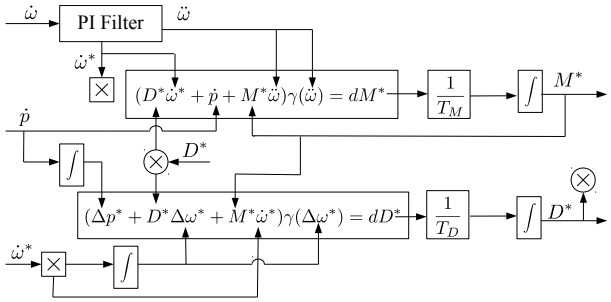

Fig. 4: Real-time loop for inertia estimation (21)-(22).

IV. Case Study

The WSCC 9-bus system shown in Fig. 5 is utilized in this section to investigate the performance and accuracy of the proposed on-line inertia and damping estimators. To test the performance of the estimators with SGs, the standard WSCC 9-bus system described in [27] is used. Then the machine connected at bus 2 is substituted for a VSG and a Doubly-Fed Induction Generator (DFIG) to test the estimation of equivalent inertia constant and droop gains of non-synchronous devices.

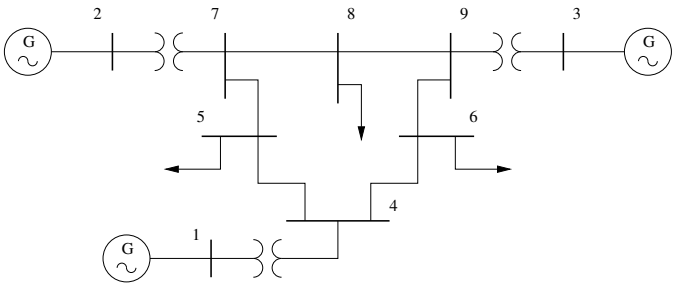

Fig. 5: WSCC 9-bus system.

This section considers and compares three on-line inertia estimators. The estimators are denoted as E0 based on (8), E1 based on (11) (see Fig. 2) and E2 based on (21)-(22) (see Fig. 4). Three different devices are considered with the following objectives:

1) Verify the accuracy of the proposed estimators to evaluate the inertia constant of SGs;
2) Test the accuracy of the estimators on tracking the constant and time-varying inertia of the grid-forming CIG via a VSGs with known inertia;
3) Illustrate the capability of the estimators to evaluate the inertia support from the stochastic renewable source, i.e. the WPP, without and with co-located Energy Storage System (ESS) in grid-following control.

All scenarios are triggered by a sudden load change, i.e. an increase of 20% load connecting to Bus 5, occurring at $t = 1$ s. The thresholds $\epsilon_o = \epsilon_p = \epsilon_{\ddot{\omega}} = \epsilon_{\Delta\omega} = 10^{-6}$ are used in Section IV-A and IV-B. The time step for all time domain simulations is 1 ms. This is also assumed to be the sampling time of the measurements utilized in the proposed estimators. All simulations are obtained using the Python-based software tool Dome [28].

A. Inertia estimation for SGs

This subsection discusses the performances of the on-line inertia estimators for evaluating the inertia constant of the SG connected to Bus 3 (denoted as G3). The actual mechanical starting time M_G and damping D_G of G3 are 6.02 s and 1.0 respectively. The results discussed in this section are obtained with $T_M = 0.01$ for E1, and $T_M = 0.001$ and $T_D = 0.001$ for E2.

1) No primary frequency control: In this first scenario, we assume that G3 has no TG. This is, of course, not realistic, but allows us better illustrating the transient behavior for the estimators. TGs are included in all subsequent scenarios.

Figure 6 shows the estimated mechanical starting time M_G^* of G3 through the three estimators. According to Fig. 6, both E1 and E2 can accurately estimate the inertia constant after roughly 80 ms. This period can be decreased with smaller time constants T_M, which, however, can lead to small oscillations.

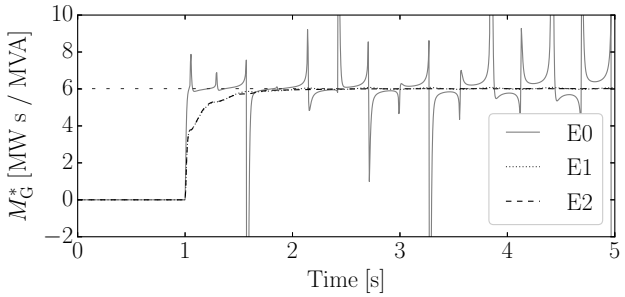

Fig. 6: Trajectories of estimated inertia of G3 without TG as obtained with E0, E1 and E2.

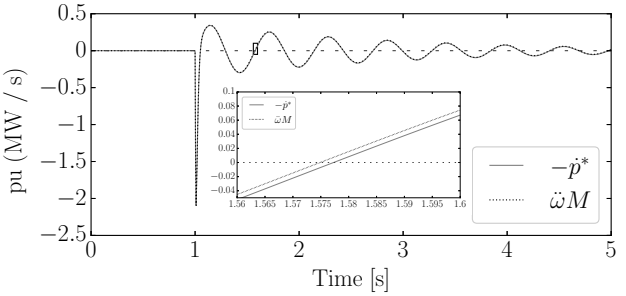

Fig. 7: Trajectories of the dynamic variations of G3 as obtained with E0.

E0 shows a faster response comparing with E1 and E2, but the worst accuracy for introducing spurious spikes. Section III-A briefly explains the cause of the spurious spikes, which can be further clarified by Fig. 7. As we can see in Fig. 7, there is a small phase differences between the nominator $-\dot{p}^*$ and denominator $\ddot{w}^*$ of (8). It means that they do not cross zero at the same time, and thus when the denominator goes to zero, the numerator is small but no null, hence the large estimation errors and, eventually, the spikes. Given the intrinsic numerical issues of E1, we consider exclusively E1 and E2 in the remainder of the paper.

2) Effect of primary frequency control: Figure 8 shows the estimated inertia of G3 with TG. In this scenario, E1 and E2 obtain the inertia constant with good accuracy. E2 shows a slightly smaller estimation error than E1.

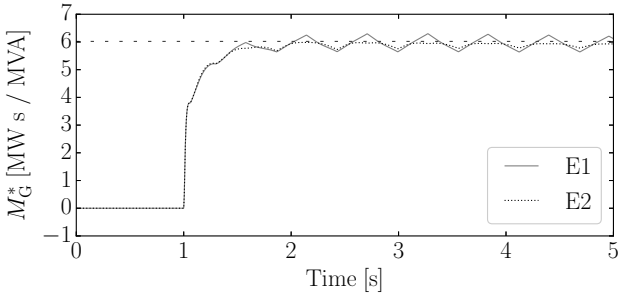

Fig. 8: Estimated inertia of G3 with TG as obtained with E1 and E2.

For the sake of example, Fig. 9 shows the estimated damping coefficient of G3 with and without TG through the estimator E2. As expected, E2 can accurately estimate the damping D of G3 only if the PFC is not included. This result is consistent with the discussion in Section III-B. Clearly, PFC is always presented in conventional power plants. But this is not a drawback of the proposed estimation approach as, in practice, the damping of synchronous machines is very small and its estimation is not necessary. Much more relevant is the estimation of the FFR droop gain of non-synchronous devices. This is discussed in Section IV-B.

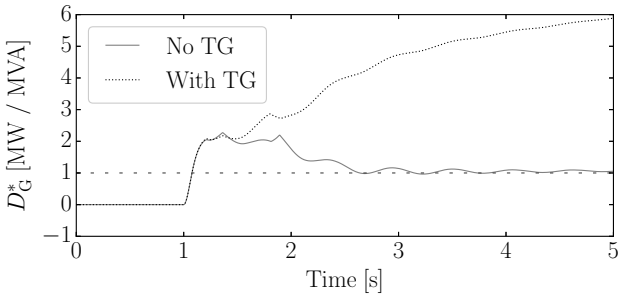

Fig. 9: Trajectories of the estimated damping of G3 with and without TG and without measurement noise as obtained with E2.

3) Impact of measurement noise: This section investigates the robustness of the proposed estimators E1 and E2 against measurement noise. Noise is added to both RoCoP and RoCoF measurements fed into the estimators. The noise is modeled as an Ornstein-Uhlenbeck stochastic process [29]. The standard deviation of the measurement noise are selected according to the expected maximum PMU error at the fundamental frequency [30] and relevant tests for RoCoP measurement [31], namely 10^{-4} for RoCoF signal and 0.01 for RoCoP signal. Figure 10 shows the inertia estimated with E1 and E2. Both estimators prove to be robust against measurement noise.

B. Inertia estimation for VSGs

The power-electronics-based VSG control is regarded as one of the most effective methods to improve the frequency

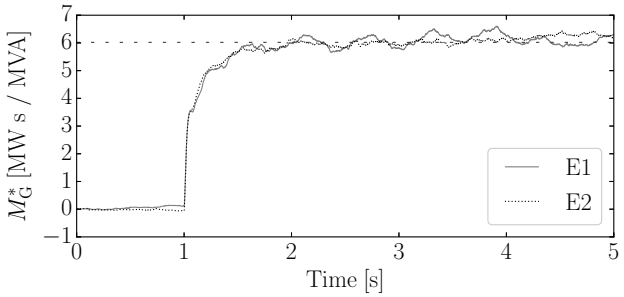

Fig. 10: Estimated inertia of G3 with TG and measurement noise as obtained with E1 and E2.

stability of the low-inertia system in recent years [1]. Since the equivalent inertia of VSGs is imposed by the control of the converter and is thus known *a priori*, the VSG represents a good test to evaluate the accuracy of the inertia estimators proposed in this work.

1) VSG with constant inertia: We first consider the VSG described in [32]. In this scenario, the inertia and FFR droop gain are constant, i.e. $M_{\mathrm{VSG}} = 20$ s and $R_{\mathrm{VSG}} = 20$.

Figure 11 shows the trajectories of the equivalent inertia as obtained with E1 with $T_M = 0.001$ and E2 with $T_M = 0.001$ and $T_D = 10^{-4}$. E2 obtains the accurate M_{VSG} roughly 60 ms after the contingency, while the estimated inertia of E1 oscillates around the actual value of the inertia. The amplitude of such an oscillation decreases as $\dot{\omega}$ decreases. This is because, in the power electronics device, the droop/damping and the inertia response "pollutes" the inertia estimation as in E1. The additional loop included in E2 for the droop/damping estimation can avoid this issue. Therefore, for the CIG with FFR, E2 performs better than E1. Since the remainder of this section focuses on CIGs, only E2 is considered.

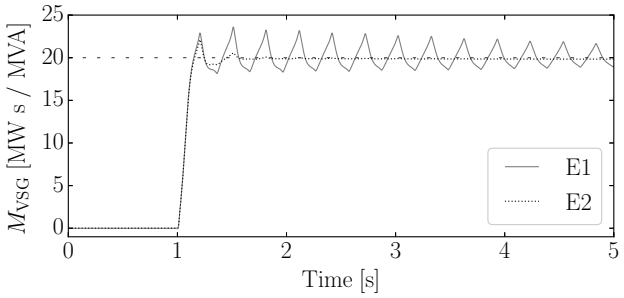

Fig. 11: Estimated inertia of the VSG with constant inertia as obtained with E1 and E2.

2) VSG with adaptive inertia: In this scenario, we consider an adaptive VSG, which can tune its inertia with respect to the grid state. The detailed model of the adaptive VSG can be found in [6]. The adaptive VSG has the same droop gain as the VSG with constant inertia discussed above.

In order to track the time-varying inertia of the adaptive VSG, we need to decrease the time constant of the estimator. A smaller time constant, however, may lead to spurious oscillations in the estimated result and thus an extra filter is needed. Figure 12 shows the trajectories of the actual inertia M of the

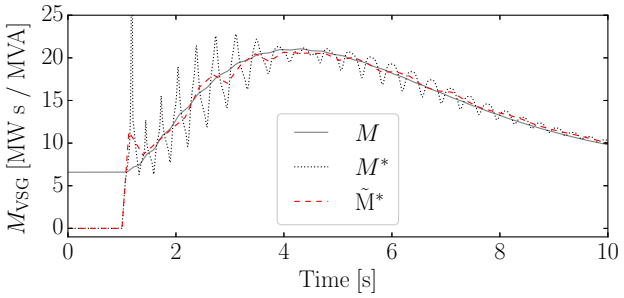

Fig. 12: Estimated inertia of the VSG with adaptive inertia as obtained with E2: M is the actual inertia of the adaptive VSG; M^* is the estimated inertia as obtained with E2; and $\tilde{M}^*$ is the filtered estimated inertia.

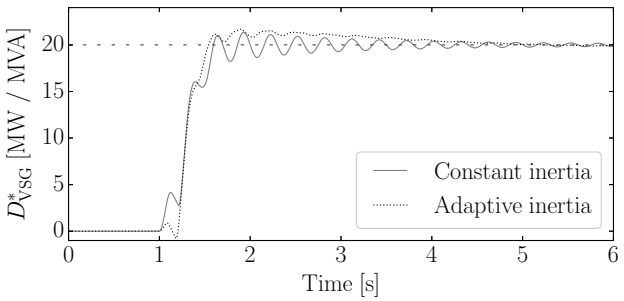

Fig. 13: Estimated droop gain of different VSGs through estimator E2 with $T_D = 10^{-4}$.

adaptive VSG, the estimated inertia M^* obtained by E2 with $T_M = 5 \cdot 10^{-5}$ s, $T_D = 10^{-4}$ s and the filtered estimated inertia $\tilde{M}^*$. The filter utilized to obtain $\tilde{M}^*$ in Fig. 12 is a basic average filter [33] with time constant $T = 0.25$ s. Figure 12 shows that the estimator E2 can accurately track the time-varying inertia with proper parameters and filter.

Figure 13 shows the estimated droop gain of the VSGs with constant and adaptive inertia through E2. E2 can accurately estimate the droop gain for these two kinds of VSG. This result is consistent with the discussion in Section III-C. The oscillations shown in the estimated inertia for adaptive VSG have no impact on the droop gain estimation.

C. Inertia estimation for WPPs

This subsection focuses on WPPs modeled as DFIGs. The detailed model of the DFIG can be found in [34]. The wind speed is modeled as an Ornstein-Uhlenbeck stochastic process that fitted with real-world wind speed measurement data [35]. The trajectories of the wind speed obtained from 500 Monte Carlo simulations. In all the figures shown in this section, μ and σ represent the mean and standard deviation of the simulated time series.

All the trajectories of the estimated inertia presented in this subsection are obtained through the estimator E2 with $T_M = 0.001$ and $T_D = 0.001$. In oder to depress the impact of the stochastic wind, we set $\epsilon_{\ddot{\omega}} = 2 \cdot 10^{-4}$ and $\epsilon_{\Delta\omega} = 0.1$.

1) WPP without ESS: We first consider the case of a DFIG without ESS. Figure 14 shows the trajectories of the output active power of the WPP following the sudden load increase. The WPP has limited response to the contingency. The active power of the WPP varies following the dynamics of the wind speed, while the mean remains the same before and after the occurrence of the contingency. Accordingly, the estimated inertia of the WPP are within the small range $M^*_{\text{WPP}} \in [-0.28, 0.1]$ and the mean is almost zero, according to Fig. 15. Figure 15 also shows that the inertia estimation is not biased by the stochastic wind dynamics resulted before the contingency. The values of $\epsilon_{\ddot{\omega}}$ and $\epsilon_{\Delta\omega}$, therefore, are adequate.

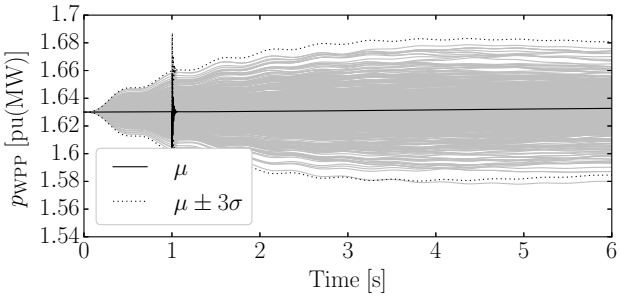

Fig. 14: Output active power of the WPP without ESS.

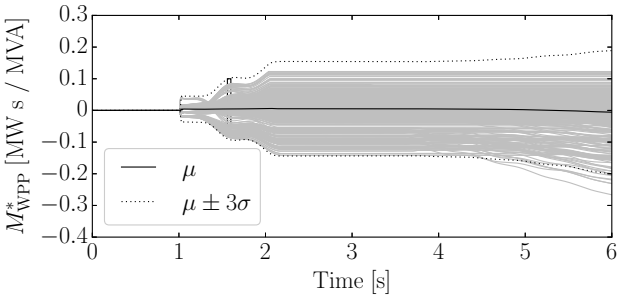

Fig. 15: Estimated inertia of the WPP without ESS.

As expected, the results shown in Figs. 14 and 15 lead to conclude that the WPP without frequency control nor ESS does not provide any significant inertia support to the system.

2) WPP with ESS: In this scenario, we consider the DFIG coupled with an ESS. The ESS is modeled as a Grid-Following Converter (GFC) with RoCoF control. The detailed model of the GFC can be found in [36]. Due to the short-term analysis, the storage limits of the ESS is not considered. The gain of the RoCoF control in the ESS is 40.

Figure 16 shows the trajectories of the output active power of the DFIG with the ESS obtained from 500 Monte Carlo simulations. The active power of the WPP with ESS increases after the occurrence of the contingency, while its magnitude vary slightly depending on the stochastic wind speed.

Figure 17 shows the estimated inertia of the WPP with ESS through the on-line inertia estimator E2 in 500 tests. Consistently with the uncertain active power injection shown in Fig. 16, the equivalent inertia provided by the WPP varies within the range $M^*_{\text{WPP}} \in [33.1, 45.8]$ according to Fig. 17. The average value of the WPP inertia is 40 s, which is consistent with the RoCoF control gain. These results indicate

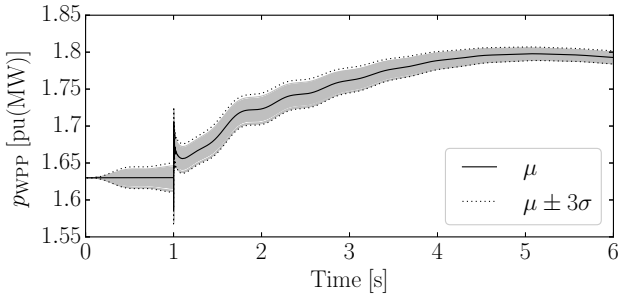

Fig. 16: Output active power of the WPP with ESS.

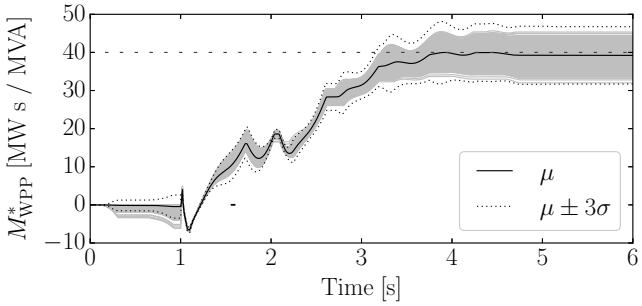

Fig. 17: Estimated inertia of the WPP with ESS.

that the WPP can provide an inertial response through the RoCoF control of its ESS.

3) Inertia estimation of SG in the high-wind-penetration system: In this scenario, we consider again the system discussed in Section IV-C.2 but, in this case, we focus on the estimation of the inertia of the synchronous generator G3 via estimator E2. Since the system includes a stochastic energy source, the thresholds are $\epsilon_{\ddot{\omega}} = 2 \cdot 10^{-4}$ and $\epsilon_{\Delta\omega} = 0.1$, and the time constants are $T_M = T_D = 0.001$ s.

Figure 18 shows the estimated inertia of G3 in the revised WSCC 9-bus system with high wind penetration and FFR energy storage through the on-line inertia estimator E2 obtained with 500 simulations. E2 shows a satisfactory accuracy, even though small fluctuations are introduced compared to the ideal scenario discussed in Section IV-A. In the vast majority of Monte Carlo realizations, the thresholds avoid to trigger the inertia estimation before the occurrence of the contingency. In general, thus, and as shown in Fig. 18, the accuracy of inertia estimation following the contingency is not affected by noise. These results also demonstrate that E2 is able to obtain an accurate estimation of the inertia of a specific device even if the system include other devices with faster dynamics and controllers.

V. Conclusion

This paper elaborates on the inertia estimation method (E0) discussed in [20] and proposes two on-line inertia estimation formulas for both synchronous and non-synchronous devices. The first proposed method (E1) avoids the potential numerical issues of E0 by changing the structure of the formula. The second method (E2) further improves the accuracy of E1 by including an additional equation to eliminate the effect of

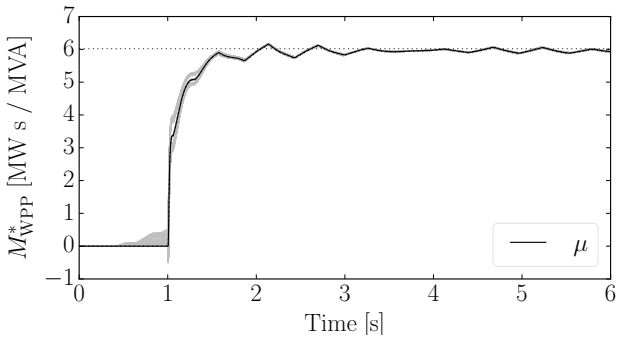

Fig. 18: Estimated inertia of G3 in the modified WSCC 9-bus system with inclusion of a WPP and an ESS.

damping and/or droop. E1 is simpler and shows satisfactory accuracy for the inertia estimation of the SG. On the other hand, E2 works better for non-synchronous devices, including time-varying inertia response and stochastic sources.

The work presented in this paper can be extended in various directions. We aim at further validating the proposed inertia estimation using measurements of real-world grids. We also aim at improving its robustness against large measurement errors, due to, e.g., cyber attacks. We will explore other applications of the proposed estimators, e.g., tracking the inertia of sub-networks rather than single devices. This can done by modeling the sub-network as a multi-port device. Finally, we are considering the development of advanced controllers that track the inertia by means of the estimators proposed in this work.

References

[1] F. Milano, F. Dörfler, G. Hug, D. J. Hill, and G. Verbič, "Foundations and challenges of low-inertia systems (invited paper)," in *2018 Power Systems Computation Conference (PSCC)*, 2018, pp. 1–25.

[2] H. Gu, R. Yan, and T. K. Saha, "Minimum synchronous inertia requirement of renewable power systems," *IEEE Trans. on Power Systems*, vol. 33, no. 2, pp. 1533–1543, 2018.

[3] S. D'Arco, J. A. Suul, and O. B. Fosso, "A virtual synchronous machine implementation for distributed control of power converters in smartgrids," *Electric Power Systems Research*, vol. 122, pp. 180 – 197, 2015.

[4] E. Muljadi, V. Gevorgian, M. Singh, and S. Santoso, "Understanding inertial and frequency response of wind power plants," in *2012 IEEE Power Electronics and Machines in Wind Applications*, 2012, pp. 1–8.

[5] G. S. Misyris, S. Chatzivasileiadis, and T. Weckesser, "Robust frequency control for varying inertia power systems," in *2018 IEEE PES Innovative Smart Grid Technologies Conference Europe (ISGT-Europe)*, 2018, pp. 1–6.

[6] J. Chen, M. Liu, F. Milano, and T. O'Donnell, "Adaptive virtual synchronous generator considering converter and storage capacity limits," *IEEE Trans. on Power Systems*, 2020.

[7] K. Liu and Z. Q. Zhu, "Mechanical parameter estimation of permanent-magnet synchronous machines with aiding from estimation of rotor pm flux linkage," *IEEE Trans. on Industry Applications*, vol. 51, no. 4, pp. 3115–3125, 2015.

[8] P. M. Ashton, C. S. Saunders, G. A. Taylor, A. M. Carter, and M. E. Bradley, "Inertia estimation of the GB power system using synchrophasor measurements," *IEEE Transactions on Power Systems*, vol. 30, no. 2, pp. 701–709, 2015.

[9] P. M. Ashton, G. A. Taylor, A. M. Carter, M. E. Bradley, and W. Hung, "Application of phasor measurement units to estimate power system inertial frequency response," in *2013 IEEE Power Energy Society General Meeting*, 2013, pp. 1–5.

[10] Á. G. González Rodríguez, A. González Rodríguez, and M. Burgos Payán, "Estimating wind turbines mechanical constants," in *Int. Conf. on Renewable Energy and Power Quality (ICREPQ)*, Sevilla, March 2007, p. 6977045.
[11] D. P. Chassin, Z. Huang, M. K. Donnelly, C. Hassler, E. Ramirez, and C. Ray, "Estimation of WECC system inertia using observed frequency transients," *IEEE Transactions on Power Systems*, vol. 20, no. 2, pp. 1190–1192, 2005.
[12] A. Fernández Guillamón, A. Vigueras Rodríguez, and Á. Molina García, "Analysis of power system inertia estimation in high wind power plant integration scenarios," *IET Renewable Power Generation*, vol. 13, no. 15, pp. 2807–2816, 2019.
[13] P. Wall, P. Regulski, Z. Rusidovic, and V. Terzija, "Inertia estimation using PMUs in a laboratory," in *IEEE PES Innovative Smart Grid Technologies, Europe*, 2014, pp. 1–6.
[14] V. Terzija, G. Valverde, D. Cai, P. Regulski, V. Madani, J. Fitch, S. Skok, M. M. Begovic, and A. Phadke, "Wide-area monitoring, protection, and control of future electric power networks," *Procs of the IEEE*, vol. 99, no. 1, pp. 80–93, Jan 2011.
[15] N. Petra, C. G. Petra, Z. Zhang, E. M. Constantinescu and M. Anitescu,"A Bayesian approach for parameter estimation with uncertainty for dynamic power systems," *IEEE Trans. on Power Systems*, vol. 32, no. 4, pp. 2735–2743, Jul 2017.
[16] J. Zhang and H. Xu, "Online identification of power system equivalent inertia constant," *IEEE Trans. on Industrial Electronics*, vol. 64, no. 10, pp. 8098–8107, 2017.
[17] R. K. Panda, A. Mohapatra, and S. C. Srivastava, "Application of indirect adaptive control philosophy for inertia estimation," in *2019 IEEE PES GTD Grand International Conference and Exposition Asia (GTD Asia)*, 2019, pp. 478–483.
[18] ——, "Online estimation of system inertia in a power network utilizing synchrophasor measurements," *IEEE Trans. on Power Systems*, pp. 1–1, 2019.
[19] J. Schiffer, P. Aristidou, and R. Ortega, "Online estimation of power system inertia using dynamic regressor extension and mixing," *IEEE Trans. on Power Systems*, vol. 34, no. 6, pp. 4993–5001, 2019.
[20] F. Milano and Á. Ortega, "A method for evaluating frequency regulation in an electrical grid – Part I: Theory," *IEEE Trans. on Power Systems*, accepted on July 2020, in press.
[21] Á. Ortega and F. Milano, "A method for evaluating frequency regulation in an electrical grid – Part II: Applications to non-synchronous devices," *IEEE Trans. on Power Systems*, accepted on July 2020, in press.
[22] P. Kundur, *Power System Stability And Control*. McGraw-Hill, 1994.
[23] F. Teng, M. Aunedi, D. Pudjianto, and G. Strbac, "Benefits of demand-side response in providing frequency response service in the future GB power system," *Frontiers in Energy Research*, vol. 3, p. 36, 2015.
[24] T. Kerdphol, F. S. Rahman, M. Watanabe, Y. Mitani, D. Turschner, and H. Beck, "Enhanced virtual inertia control based on derivative technique to emulate simultaneous inertia and damping properties for microgrid frequency regulation," *IEEE Access*, vol. 7, pp. 14 422–14 433, 2019.
[25] F. Milano, Á. Ortega, and A. J. Conejo, "Model-agnostic linear estimation of generator rotor speeds based on phasor measurement units," *IEEE Trans. on Power Systems*, pp. 1–1, 2018.
[26] F. Milano and Á. Ortega, "Frequency divider," *IEEE Trans. on Power Systems*, vol. 32, no. 2, pp. 1493–1501, March 2017.
[27] P. Sauer and M. Pai, *Power System Dynamics and Stability*. Prentice Hall, 1998.
[28] F. Milano, "A Python-based Software Tool for Power System Analysis," in *Procs of the IEEE PES General Meeting*, Vancouver, BC, Jul. 2013.
[29] F. Milano and R. Zárate-Miñano, "A systematic method to model power systems as stochastic differential algebraic equations," *IEEE Trans. on Power Systems*, vol. 28, no. 4, pp. 4537–4544, 2013.
[30] A. Derviškadić, P. Romano, and M. Paolone, "Iterative-interpolated dft for synchrophasor estimation: A single algorithm for p- and m-class compliant PMUs," *IEEE Trans. on Instrumentation and Measurement*, vol. 67, no. 3, pp. 547–558, 2018.
[31] F. Milano and Á. Ortega, *Frequency Variations in Power Systems: Modeling, State Estimation, and Control*. Wiley IEEE Press, 2020.
[32] J. Chen, M. Liu, and T. O'Donnell, "Replacement of synchronous generator by virtual synchronous generator in the conventional power system," in *IEEE PES General Meeting (PESGM)*, Atlanta, GA, USA, 2019, pp. 1–5.
[33] Y. Pititeeraphab, T. Jusing, P. Chotikunnan, N. Thongpance, W. Lekdee, and A. Teerasoradech, "The effect of average filter for complementary filter and kalman filter based on measurement angle," in *2016 9th Biomedical Engineering International Conference (BMEiCON)*, 2016, pp. 1–4.
[34] F. Milano, *Power System Modelling and Scripting*. London: Springer, 2010.
[35] G. M. Jónsdóttir and F. Milano, "Data-based continuous wind speed models with arbitrary probability distribution and autocorrelation," *Renewable Energy*, vol. 143, pp. 368 – 376, 2019.
[36] M. P. N. van Wesenbeeck, S. W. H. de Haan, P. Varela, and K. Visscher, "Grid tied converter with virtual kinetic storage," in *IEEE PowerTech*, 2009, pp. 1–7.

Muyang Liu (S'17-M'20) received the ME and Ph.D. in Electrical Energy Engineering from University College Dublin, Ireland in 2016 and 2019. Since December 2019, she is a senior researcher with University College Dublin. Her scholarship is funded through the SFI Investigator Award with title "Advanced Modeling for Power System Analysis and Simulation." Her current research interests include power system modeling and stability analysis.

Junru Chen (S'17-M'20) received the ME and Ph.D. degree in Electrical Energy Engineering from University College Dublin in 2016 and 2019. He was exchanging student at Kiel University (Germany) in 2018 and at Tallinn University of Technology (Estonia). He is currently a senior researcher at University College Dublin and a visiting scholar at Aalborg University, Denmark. His current research interests in Power electronics control, modeling, stability and application.

Federico Milano (S'02, M'04, SM'09, F'16) received from the University of Genoa, Italy, the ME and Ph.D. in Electrical Engineering in 1999 and 2003, respectively. From 2001 to 2002, he was with the Univ. of Waterloo, Canada. From 2003 to 2013, he was with the Univ. of Castilla-La Mancha, Spain. In 2013, he joined the Univ. College Dublin, Ireland, where he is currently Professor of Power Systems Control and Protections and Head of Electrical Engineering. His research interests include power systems modeling, control and stability analysis.